ACS OMEGA

http://pubs.acs.org/journal/acsodf

Article

Calotropis Gigantea Fiber—A Biogenic Reinforcement Material for Europium Substituted Hydroxyapatite/Poly(3,4-propylenedioxythiophene) Matrix: A Novel Ternary Composite for Biomedical Applications

Ramachandran Raji, Shinyjoy Elangomannan, Ramya Subramani, Kavitha Louis, Manoravi Periasamy, and Gopi Dhanaraj*

Cite This: *ACS Omega* 2022, 7, 6024–6034

Read Online

ACCESS | Metrics & More | Article Recommendations

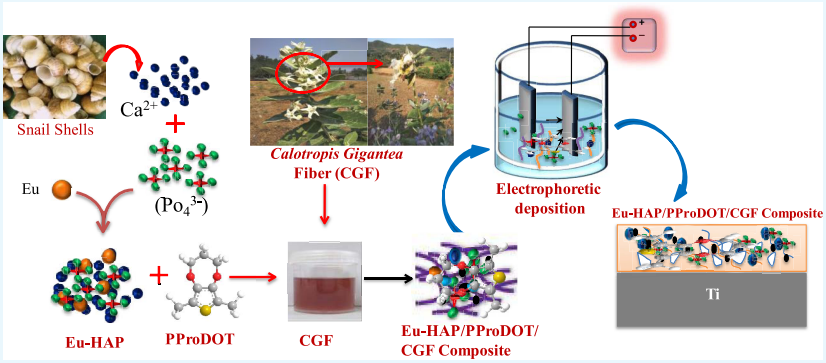

ABSTRACT: Novel multifunctional biocomposite materials that mimic the properties of bone are the need of the hour. In view of this, the current work is focused on the fabrication of a snail shells derived europium-substituted hydroxyapatite (Eu-HAP)/poly(3,4-propylenedioxythiophene) (PProDOT)/*Calotropis gigantea* fiber (CGF) ternary composite on titanium (Ti) for biomedical applications. The structural, morphological, mechanical, electrochemical, and biological properties of the as-developed coatings on Ti were characterized. The obtained results clearly confirmed the formation and properties of the ternary composite (Eu-HAP/PProDOT/CGF). The presence of CGF, an exceptional reinforcement material, in the ternary composite is proven to improve mechanical and biological properties compared to other coatings (i.e., coating without CGF). Also, electrochemical studies revealed better anticorrosion properties of the composite-coated Ti in a simulated body fluid (SBF) solution. Similarly, the presence of Eu-HAP and PProDOT in the composite is clearly evident from the antibacterial activity against *Staphylococcus aureus* (*S. aureus*) and *Escherichia coli* (*E. coli*) and also by the cell proliferation and cell adhesion by the MTT assay test. Thus, we suggest that the fabricated Eu-HAP/PProDOT/CGF ternary composite with mechanical, corrosion resistance, and biocompatible properties might be an appropriate candidate for biomedical applications.

INTRODUCTION

Bone fractures or bone defects due to trauma, tumors, or skeletal disorders have become one of the global issues and a formidable challenge in the field of orthopedics.[1,2] Hence, the fabrication of a perfect bone repair material is an immense need for a promising approach toward bone repair and regeneration.[3−5] An ideal bone replacement material must possess excellent biocompatibility and suitable mechanical properties to mimic the bone. In fact, the natural bone is a composite material consisting of inorganic (60%) and organic (30%) mineral phases and water (10%).[6,7] Hydroxyapatite ($Ca_{10}(PO_4)_6(OH)_2$, HAP) is the major inorganic component of bone that has wide biomedical applications because of its osteoconductive and biocompatible properties.[8−10] HAP can be prepared by various methods like the precipitation method, template-assisted method, sol−gel method, etc.[11−13] HAP can be prepared chemically, or it can be extracted from natural sources. However, the synthetic method of HAP preparation involves the utilization of high-purity chemical reagents.

Received: November 12, 2021
Accepted: January 28, 2022
Published: February 10, 2022

https://doi.org/10.1021/acsomega.1c06372
ACS Omega 2022, 7, 6024−6034

Comparatively, the HAP synthesized through natural sources was found to be more similar to the human bone because of the presence of trace elements like Na^+, Zn^{2+}, Mg^{2+}, K^+, etc. Hence, nowadays, HAP is synthesized from natural materials.[14] The naturally plentiful snail-shell waste is selected for the preparation of HAP because of its easy availability and low cost.[15] Snail shells (SS) are marine exoskeletons, which are composed of calcium carbonate ($CaCO_3$) and other organic components ($MgCO_3$).[16] Inadequate studies have been attempted on the synthesis of HAP using snail shells as a calcium source.[17,18] Moreover, the substitution of Ca^{2+} ions with various bioactive ions such as Mg^{2+}, Zn^{2+}, Mn^{2+}, Sr^{2+}, Ag^{2+}, Ba^{2+} Y^{3+}, La^{3+}, Sm^{3+}, $Ce^{3+,}$ Eu^{3+}, etc., enhances the biological properties of HAP. The minerals substituted in HAP will enhance cell adhesion and proliferation of osteoblast cells, improve bioactivity, and provide excellent antimicrobial activity.[19−21] The trivalent cations are reported to exhibit improved biocompatibility and bioactive properties when compared to the divalent cations. Cell adhesion and proliferation were also found to be increased with the ions substituted in HAP.[22] Hence, in this study, Eu^{3+} is substituted in HAP to enhance the biocompatibility. However, the intrinsic brittleness, low fracture toughness, and low wear resistance of HAP make it unsuitable for long-term applications.[23,24]

To overcome these limitations, it is essential to develop HAP-based biocompatible composite materials without causing adverse effects to humans. In recent years, the incorporation of polymers into HAP has proven to be a promising alternative in biomedical applications.[25] In particular, the conductive polymer (CP) has been a subject of intense research because of its facile preparation process, light weight, corrosion resistance properties, etc. Recently, the conducting polymer poly(3,4-propylenedioxythiophene) (PProDOT) has been considered to be the potential polymer due to its high conductivity, special physical and chemical properties, excellent stability, excellent biocompatibility, nontoxicity, and biodegradability.[26,27] Thus, the HAP incorporated into the polymer has shown an improved interface and enhanced cell adhesion to the biological environment.[28] To endow the composite with mechanical rigidity and exceptional biocompatibility, the incorporation of suitable reinforcing materials such as Al_2O_3, Y_2O_3, ZrO_2, yttria-stabilized zirconia (YSZ), silk fibers and cellulose fibers, carbon nanotubes (CNTs), carbon nanofibers (CNFs), TiO_2, and graphene oxide (GO) is adopted.[29−32]

Over the past few decades, fiber (synthetic)-reinforced composite has acquired great attention in the field of bone regeneration and several other biomedical applications.[33−35] Most of the synthetic fibers are expensive and toxic, which would inevitably cause severe problems that may even lead to a second surgery when not used in an appropriate way. However, the use of natural fibers, such as bamboo, jute, hemp, banana, *Calotropis gigantea*, etc., as reinforcing materials for the composite, has attracted much interest among researchers. Among the natural fibers, *C. gigantea* fiber (Family: Asclepiadaceae) is a natural fiber, which consists of 66% cellulose, 8−9% lignin, 1.8−3% wax, 3% pectin, and 21% hemicelluloses. This fiber possesses the characteristics of excellent biocompatibility and nontoxicity.[36−38] CGF finds its application chiefly in the textile industry as a raw material with intrinsic biodegradability, and to date, only very few studies on CGF-reinforced composites have been carried out.[39] The fibers can be obtained from the fruits of the plant and then used in the fabrication of the composite. The cost for the formation of the fiber-based composite is very cheap since the fiber is naturally available.[40] But, the hydrophilic nature of the fiber restricts its application in load-bearing applications, i.e., the nonuniform dispersion of the fiber and the lack of interfacial bonding reduce the quality of the ternary composite. To overcome these defects, surface modifications of the fiber, such as chemical treatment, alkali treatment, etc., are adopted to enhance the adhesion of fiber to the matrix. The surface treatment will provide the complete removal of any surface impurities and other noncellulosic material. The functional groups on the surface of the fibers will induce the formation of HAP, which acts as a bridge between the fiber and the polymer. Since there were no investigations on the reinforcement of CGF into the polymer and HAP matrix, the authors made an attempt to explore the possibility of using CGF stem bark fiber as a new reinforcing material in the polymer/Eu-HAP composite. Thus, a ternary composite (Eu-HAP/PProDOT/CGF) combining the advantages of ceramic, polymer, and fiber with improved mechanical and biological properties will be a suitable coating material for metallic implants used in orthopedic applications.

In general, a biomaterial is known to improve the quality of life and the range of its application is vast, which includes bone substitutes like Ti and its alloys, magnesium alloys, 316L stainless steels, Co−Cr alloys, etc. In the present work, the authors have developed the ternary composite over Ti because of its light weight, acceptable biocompatible properties, reasonable corrosion resistivity, and ease of fabrication.[41,42] Several deposition techniques were used for the fabrication of the ternary composite coating on metallic implants.[43−45] Electrophoretic deposition is the most viable method as it involves a very simple setup, low-cost equipment, and an easy-to-achieve homogeneous coating on metallic implants. Thus, we utilized this method to fabricate the ternary composite on Ti for biomedical implant applications. This ternary composite would have the beneficial properties of each added component by complementing their shortcomings, thereby yielding an outstanding material with excellent mechanical, corrosion resistance, and biocompatible properties for biomedical implant applications, especially in the field of orthopedics.

RESULTS AND DISCUSSION

Fourier Transform Infrared (FTIR) Analysis. The FTIR spectra of HAP, Eu-HAP, Eu-HAP/PProDOT, and the Eu-HAP/PProDOT/CGF ternary composite are shown in Figure 1a−d. The spectrum for HAP (Figure 1a) shows the peaks corresponding to the stretching and bending modes of the hydroxyl group at 1572, 1162, 722, and 492 cm^{-1}. The absorption peaks for the phosphate (PO_4^{3-}) groups of HAP were observed at 1410, 1027, 610, 559, and 450 cm^{-1}. The FTIR spectrum for the Eu-substituted HAP is shown in Figure 1b, which also exhibits peaks similar to HAP with slight variations in the wavenumbers for PO_4^{3-} and OH^- groups. This slight shift in the peaks for Eu-HAP compared to HAP clearly evidences the substitution of Eu in the Ca lattice of HAP. Figure 1c shows the spectrum of the Eu-HAP/PProDOT composite with the peaks corresponding to both Eu-HAP and PProDOT.

The characteristic peaks located at 1033, 611, and 491 cm^{-1} are assigned to the phosphate groups of Eu-HAP, whereas the peak at 3458 cm^{-1} corresponds to the OH group of Eu-HAP.[55]

https://doi.org/10.1021/acsomega.1c06372
ACS Omega 2022, 7, 6024−6034

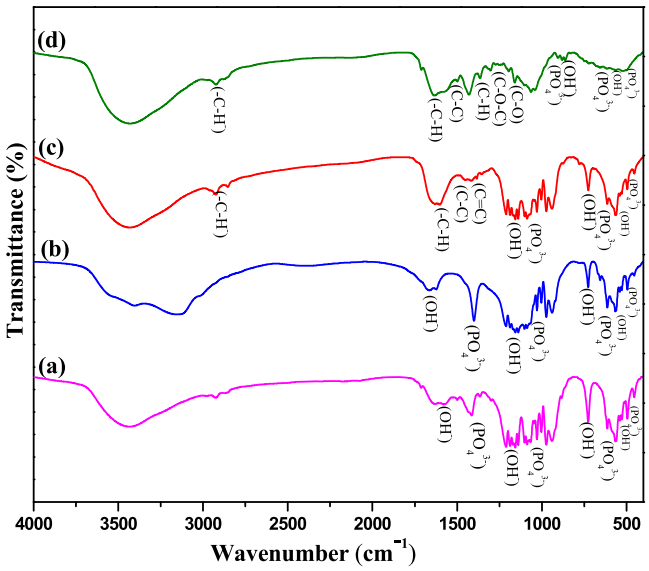

Figure 1. FTIR spectra of (a) HAP, (b) Eu-HAP, (c) Eu-HAP/PProDOT, and (d) Eu-HAP/PProDOT/CGF composite coatings.

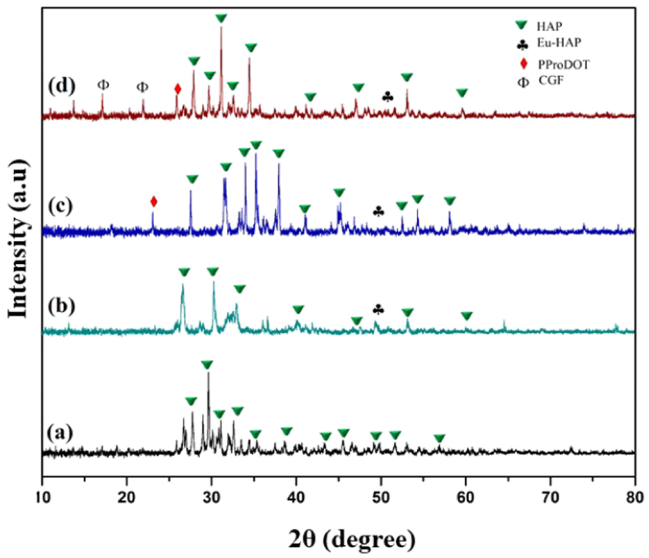

Figure 2. XRD patterns of (a) HAP, (b) Eu-HAP, (c) Eu-HAP/PProDOT, and (d) Eu-HAP/PProDOT/CGF composite coatings.

The peaks at 2922 and 1596 cm^{-1} represent the C−H stretching, whereas the peaks found at 1438 and 1378 cm^{-1} correspond to the C−C and C═C groups of PProDOT, respectively.

The FTIR spectrum of the Eu-HAP/PProDOT/CGF ternary composite is shown in Figure 1d. The spectrum exhibits the peaks related to Eu-HAP, PProDOT, and CGF. Along with the peaks for the PProDOT and Eu-HAP, the peaks related to CGF, i.e., C−O−C and C−O, are present at 1265 and 1155 cm^{-1}, respectively. Compared with the spectra of CGF and Eu-HAP/PProDOT, the spectrum of the Eu-HAP/PProDOT/CGF ternary composite (Figure 1d) demonstrates that neither peak shifts nor new absorption peaks were identified with the addition of CGF, suggesting that the composites are a mixture of these three compounds without forming identifiable new interfacial chemical bonds. This supports the formation of the Eu-HAP/PProDOT/CGF ternary composite.

X-ray Diffraction Studies. Figure 2 shows the XRD pattern for HAP, Eu-HAP, Eu-HAP/PProDOT, and Eu-HAP/PProDOT/CGF. The XRD pattern of HAP is shown in Figure 2a, in which the diffraction peaks are observed at 2θ values of 26.72, 29.62, 31.1, 32.57, 35.43, 38.63, and 43.31°, which is in good agreement with the standard database of the International Centre for Diffraction Data (ICDD card no. 09-0432).

The Eu-HAP coating also exhibited peaks similar to HAP with slight shifts in the 2θ values, which are evident from the XRD pattern, as depicted in Figure 2b, and the obtained patterns for Eu-HAP coincide well with the standard ICDD value. This slight shift in the XRD patterns is due to the substitution of Eu in HAP.[56,57] The ionic radius of the Eu^{3+} (1.07 Å) is not much higher than that of Ca^{2+} (0.99 Å) because the substitution of ions such as Eu^{3+} did not influence the XRD pattern of Eu-HAP.

Figure 2c shows the XRD pattern for the Eu-HAP/PProDOT composite. The strong diffraction peaks at 2θ values of 31.43, 33.98, 35.24, 37.94, and 41.16° are attributed to Eu-HAP and no other secondary peaks were found, whereas the remaining peaks at 23.07 and 27.53° were assigned to PProDOT.[58] The major diffraction peaks identified for the Eu-HAP are in good agreement with the standard data for HAP (ICDD card No. 09-0432), whereas for the Eu-HAP (Figure 2b), the diffraction peak positions shifted toward the lower angles from the standard XRD patterns for HAP, indicating the substitution of Eu into the pure HAP sample.[57] These peaks confirm the formation of the Eu-HAP/PProDOT composite, as shown in Figure 2c. Along with the peaks for the Eu-HAP and PProDOT, the diffraction angle at 17.08 and 21.91° confirms the presence of CGF in the ternary composite (Figure 2d). As a result, the patterns of the Eu-HAP/PProDOT/CGF ternary composite illustrate that no appreciable new interfacial crystalline phases were lost or formed with the addition of CGF and PProDOT.

Morphological Analysis. To examine the changes in the structure of the as-developed coatings, the morphological analysis was carried out for HAP, Eu-HAP, Eu-HAP/PProDOT, and Eu-HAP/PProDOT/CGF composite coatings using the SEM technique, and the corresponding images are shown in Figure 3a−d. The elemental composition of the coatings was examined by the EDAX analysis and is shown in Figure 3a′−d′. The morphology of the HAP coating is found to be aggregated with irregular grainlike structures over the surface, as shown in Figure 3a. The substitution of Eu in HAP resulted in a change in the morphology, i.e., the grainlike structure completely covered the entire surface, thereby providing a compact coating over the Ti metal, which can be clearly seen in Figure 3b.

The surface morphology of the Eu-HAP/PProDOT matrix (Figure 3c) exhibits a smooth morphology with nonuniform aggregates of the PProDOT and Eu-HAP. Many pores were found in the Eu-HAP/PProDOT matrix morphology, which will play a major role in enhancing the formation of tissues when placed inside the body. The reinforcement of CGF in the Eu-HAP/PProDOT matrix plays a significant role in providing the desired morphology for the development of bone tissue surrounding the metallic implant (Figure 3d). Thus, these SEM results support the formation of the Eu-HAP/PProDOT/CGF ternary composite coating on Ti.

The formation of the Eu-HAP, Eu-HAP/PProDOT, and Eu-HAP/PProDOT/CGF composite coatings over the Ti is

https://doi.org/10.1021/acsomega.1c06372
ACS Omega 2022, 7, 6024−6034

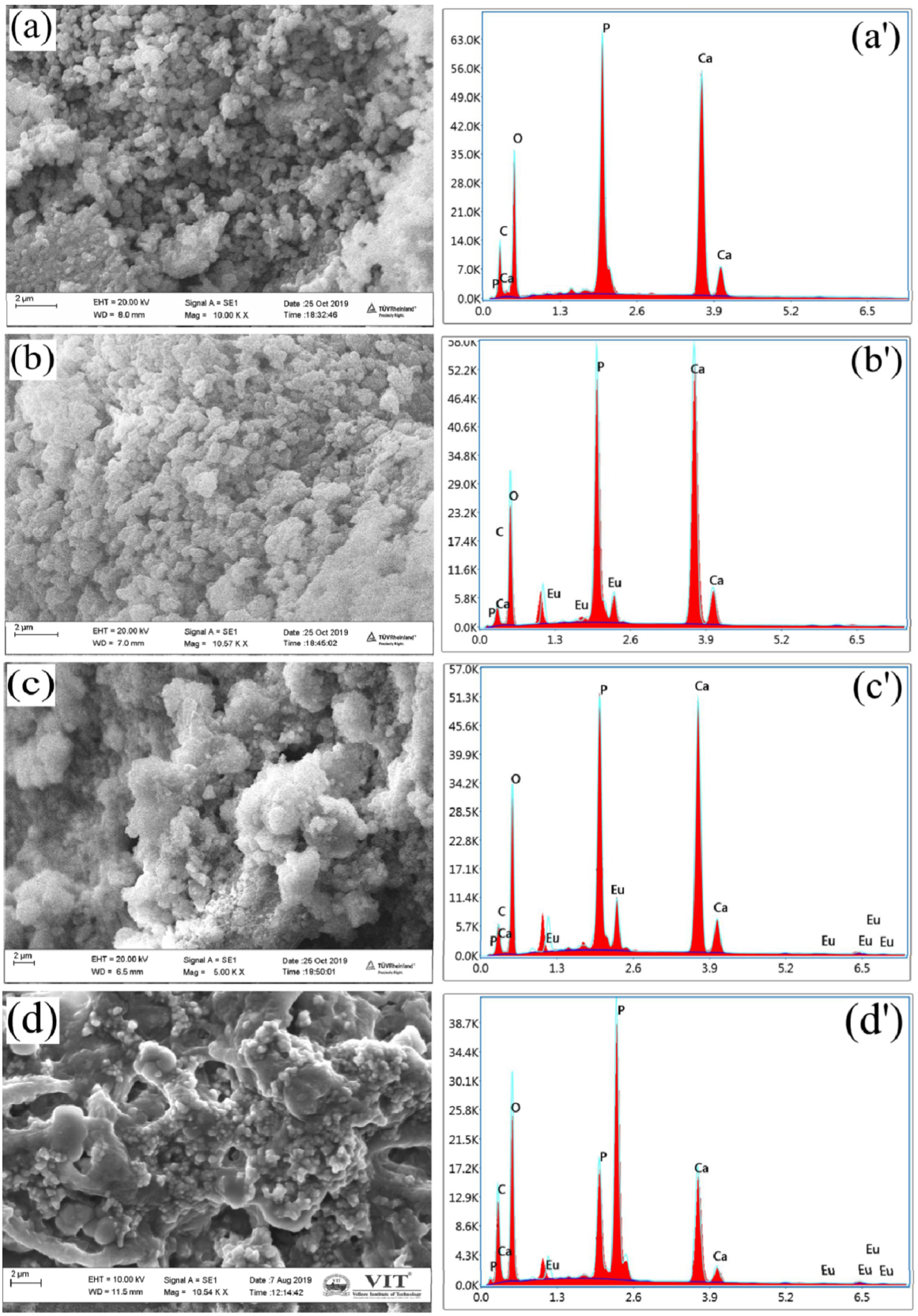

Figure 3. SEM morphology and EDX spectra of (a, a′) HAP (b, b′), Eu-HAP (c, c′), Eu-HAP/PProDOT (d, d′), and Eu-HAP/PProDOT/CGF composite-coated Ti.

supported by its elemental composition by EDX analysis, as seen in Figure 3a′−d′. The presence of Ca, P, C and O confirms the formation of the HAP coating, whereas the presence of Eu along with the other peaks for HAP supports the formation of the Eu-substituted HAP, as seen in Figure 3b′. The EDX analysis of the Eu-HAP/PProDOT coating on Ti

https://doi.org/10.1021/acsomega.1c06372
ACS Omega 2022, 7, 6024−6034

(Figure 3c′) shows the presence of Ca, Eu, P, O, and C, and the Eu-HAP/PProDOT/CGF composite (Figure 3d′) reveals the presence of Ca, Eu, O, P, and C, thereby supporting the formation of the composite over Ti.

Mechanical Characterizations. The metallic implants that are to be used in a load-bearing application should exhibit excellent adhesion strength and hardness under physiological conditions. In that way, the adhesion strength of the as-fabricated coatings is of utmost significance to prove the effective function of the coating developed over Ti. The adhesion strength of the Eu-HAP-coated Ti was found to be 11.2 ± 0.6 MPa, whereas when the PProDOT was incorporated into the Eu-HAP, the value slightly increased to 15.6 ± 0.8 MPa, which shows that the poor mechanical property of the Eu-HAP is improved by the presence of PProDOT. To further enhance the mechanical property of the coated Ti to be used for load-bearing applications, a ternary composite with a suitable reinforcing material like CGF was prepared with the Eu-HAP/PProDOT matrix. The natural reinforcing material CGF-reinforced Eu-HAP/PProDOT matrix exhibited an adhesion strength of 19.4 ± 0.7 MPa, which is higher than that obtained with other coatings on Ti. Thus, from the adhesion strength values (Figure 4a), it can be clear that the ternary composite-coated Ti will be a potential candidate for load-bearing orthopedic applications. Similarly, the hardness of the coating is also essential for various biomedical applications. The microhardness value was found to be 356.2 ± 1.8 Hv for Eu-HAP, 398 ± 3.2 Hv for Eu-HAP/PProDOT, and 450.4 ± 5 Hv for Eu-HAP/PProDOT/CGF (Figure 4b).

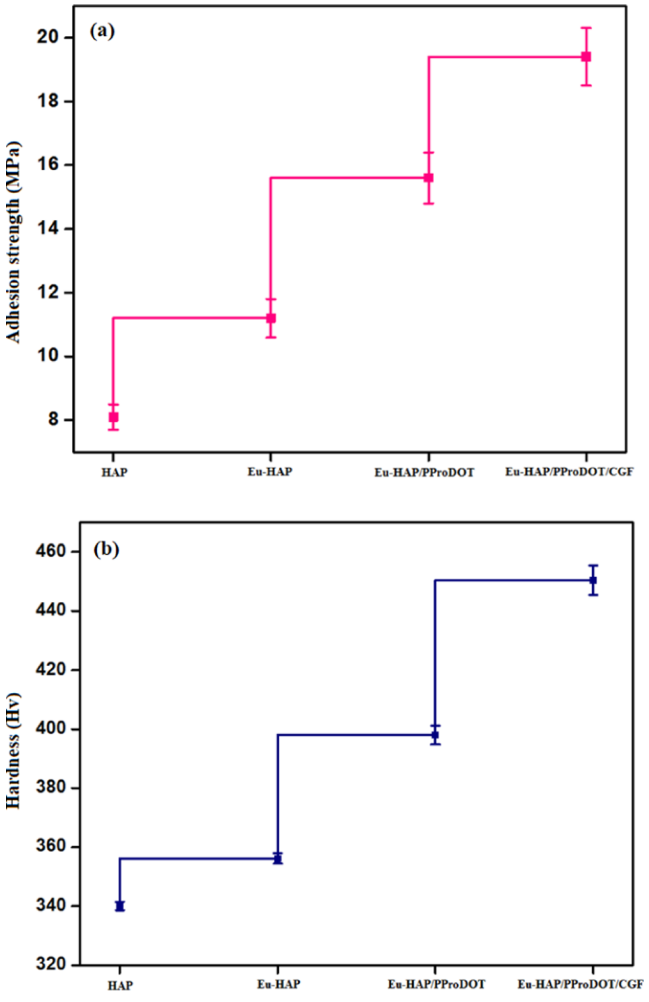

Figure 4. (a) Adhesion strength and (b) hardness of HAP, Eu-HAP, Eu-HAP/PProDOT, and Eu-HAP/PProDOT/CGF composite-coated Ti.

The ternary composite-coated Ti exhibits the highest hardness value, which renders it more suitable for load-bearing orthopedic implant applications. Thus, from this mechanical characterization of the coating, the role of CGF as a reinforcing material in providing an excellent mechanical property to the coating is clearly manifested.

Potentiodynamic Polarization Measurements. The electrochemical characterization of the as-developed coating is very essential to evaluate the anticorrosion behavior of the coated metallic implants when used in biomedical applications. The electrochemical parameters like corrosion potential (E_{corr}) and corrosion current density (i_{corr}) were evaluated in an SBF solution, and the plots corresponding to the uncoated Ti and coated Ti are shown in Figure 5 and the values are shown in Table 1.

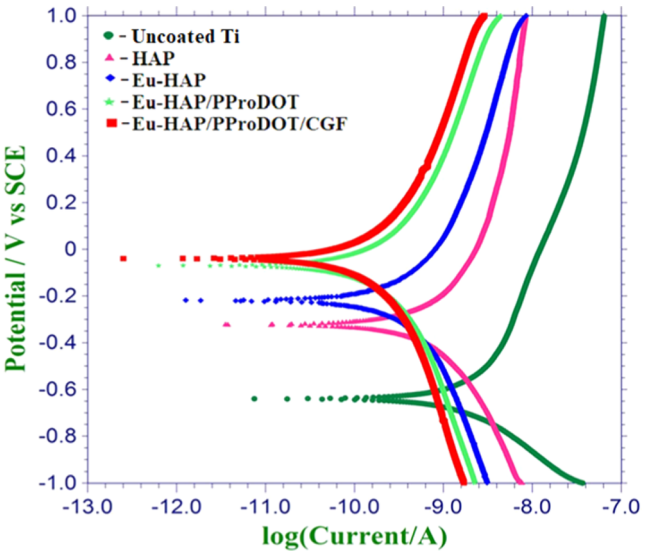

Figure 5. Potentiodynamic polarization curves of uncoated Ti, HAP, Eu-HAP, Eu-HAP/PProDOT, and Eu-HAP/PProDOT/CGF composite-coated Ti.

Table 1. Electrochemical Parameters of the Uncoated and Coated Ti in an SBF Solution

sample code	E_{corr} (V vs SCE)	i_{corr} (μA cm^{-2})
uncoated Ti	−0.638 ± 0.003	3.648 ± 0.7
HAP	−0.325 ± 0.007	1.278 ± 0.5
Eu-HAP	−0.217 ± 0.004	0.550 ± 0.03
Eu-HAP/PProDOT	−0.073 ± 0.005	0.267 ± 0.02
Eu-HAP/PProDOT/CGF	−0.041 ± 0.002	0.216 ± 0.04

The E_{corr} values of the uncoated Ti, HAP, Eu-HAP, Eu-HAP/PProDOT, and Eu-HAP/PProDOT/CGF were found to be −0.638 ± 0.003, −0.325 ± 0.007, −0.217 ± 0.004, −0.073 ± 0.005, and −0.041 ± 0.0052 V, respectively. Also, as seen in the curves, the obtained values show that the Eu-HAP/PProDOT/CGF ternary composite-coated Ti exhibited higher corrosion resistance, which could be well evident from the E_{corr} values. It can be well explained that the maximum shift toward

https://doi.org/10.1021/acsomega.1c06372
ACS Omega 2022, 7, 6024−6034

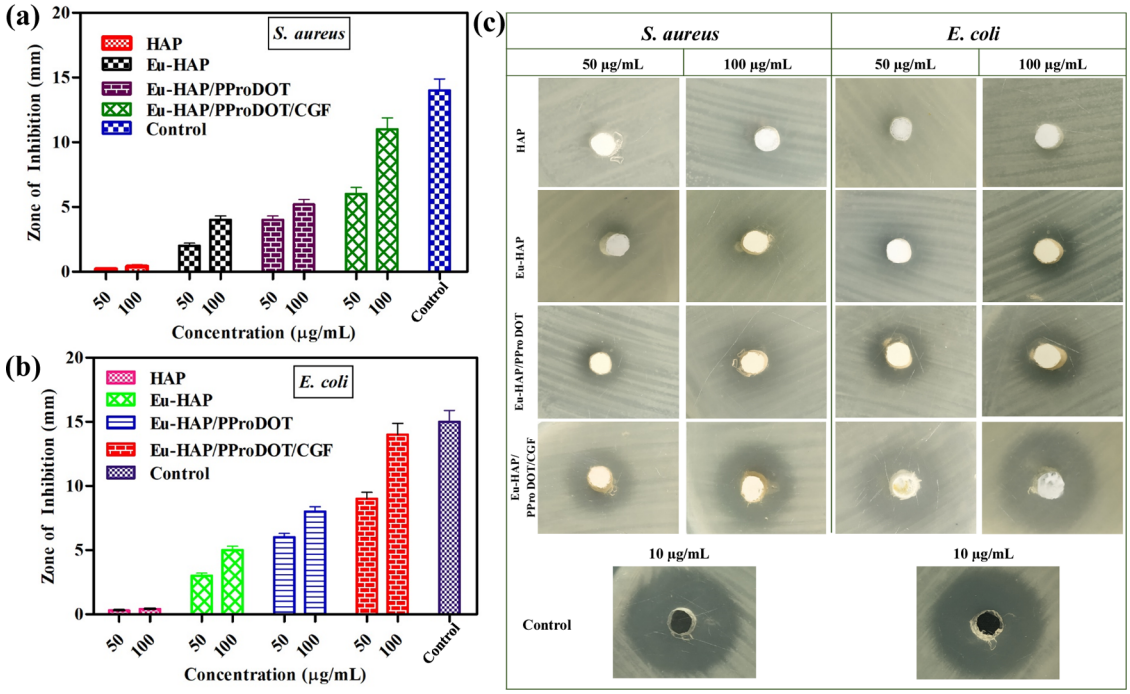

Figure 6. Bar diagram (a, b) and plates (c) showing the antibacterial activity of HAP, Eu-HAP, Eu-HAP/PProDOT, and Eu-HAP/PProDOT/CGF composites against *S. aureus* and *E. coli*.

the noble direction is a clear sign of higher anticorrosion properties in an SBF solution.

Further, with respect to the i_{corr} values, the ternary composite (i_{corr} value 0.216 ± 0.04 μA cm^{-2}) showed a lower value compared to other coatings on Ti. Thus, the increased E_{corr} and decreased i_{corr} values for the Eu-HAP/PProDOT/CGF ternary composite-coated Ti supports the anticorrosion property of the composite in the physiological medium and also confirms the corrosion protective nature of the as-developed Eu-HAP/PProDOT/CGF composite coating.

Antibacterial Activity. The metallic implants are easily prone to infection when used in the physiological medium, i.e., when placed inside the body. Hence, for this purpose, antibiotics are used, which are often not effective. The antibacterial agents like Eu are substituted in the ceramic coating and were found to improve the antibacterial property of the coatings. The bar diagram (Figure 6a,b) shows the antibacterial activity of the HAP, Eu-HAP, Eu-HAP/PProDOT, and Eu-HAP/PProDOT/CGF composite coating evaluated against the Gram-positive (*S. aureus*) and Gram-negative (*E. coli*) bacteria at 50 and 100 μg/mL of the coatings, and the corresponding antibacterial plates exposing the zone of inhibition are shown in Figure 6c. Also, for the Eu-HAP/PProDOT/CGF ternary composite, the measured inhibition zones for *S. aureus* and *E. coli* were found to be 10 and 11 mm for 50 and 100 μg/mL and 13.5 and 14.5 mm for 50 and 100 μg/mL, respectively. It is clear that among the HAP, Eu-HAP, Eu-HAP/PProDOT, and Eu-HAP/PProDOT/CGF ternary composite coatings, the antibacterial activity was found to be more for the ternary composite coating and especially against the *E. coli,* which is evaluated by measuring the zone of inhibition around the coating material.

The Eu-HAP/PProDOT/CGF ternary composite exhibited an excellent antibacterial activity at 100 μg/mL, which could be mainly due to the substitution of Eu in HAP and also due to the presence of CGF in the composite. This is further confirmed by the plates shown in Figure 6c. The coating materials interact with the cell wall of bacteria, thereby causing structural damage, which then affects bacterial growth. The difference in the antibacterial activity of the coating against the two bacterial strains is due to the difference in the cell wall of *S. aureus* and *E. coli*.

***In Vitro* Cell Viability.** The *in vitro* cell viability of HOS MG63 cells on different concentrations of (12.5, 25, 50, 100, and 200 μg/mL) HAP, Eu-HAP, Eu-HAP/PProDOT, and the Eu-HAP/PProDOT/CGF ternary composite was evaluated with respect to control at 5 days of incubation.

The optical density values for the HOS MG63 cells measured through formazan solutions are shown in Figure 7a in terms of percentage cell viability. Comparatively, the Eu-HAP/PProDOT/CGF ternary composite exhibited greater cell viability compared with other samples. The viability of the cells was significant for the composite samples treated with concentrations of 12.5 μg/mL (98%). On further increasing the sample concentration to 25 and 50 μg/mL, considerable cell viabilities of 96 and 94%, respectively, were observed. In addition, the increasing concentration of 100 and 200 μg/mL illustrates a saturation in the cell viability of 90 and 89%. This saturation of cell viability also reveals that the samples with higher concentrations are highly biocompatible without any cytotoxicity. Based on these results, the Eu-HAP/PProDOT/CGF ternary composite exhibited nontoxicity to the cell lines at 5 days of incubation.

The obtained % cell viability is further substantiated by their corresponding optical microscopy images, as shown in Figure 7b. The Eu-HAP/PProDOT/CGF ternary composite at a sample concentration of 12.5 μg/mL exhibited appreciable cell viability of HOS MG63 cells. The optical microscopy images show the presence of viable cells at different concentrations. Even the higher concentrations of 200 μg/mL of the Eu-HAP/PProDOT/CGF ternary composite revealed the presence of a

https://doi.org/10.1021/acsomega.1c06372
ACS Omega 2022, 7, 6024−6034

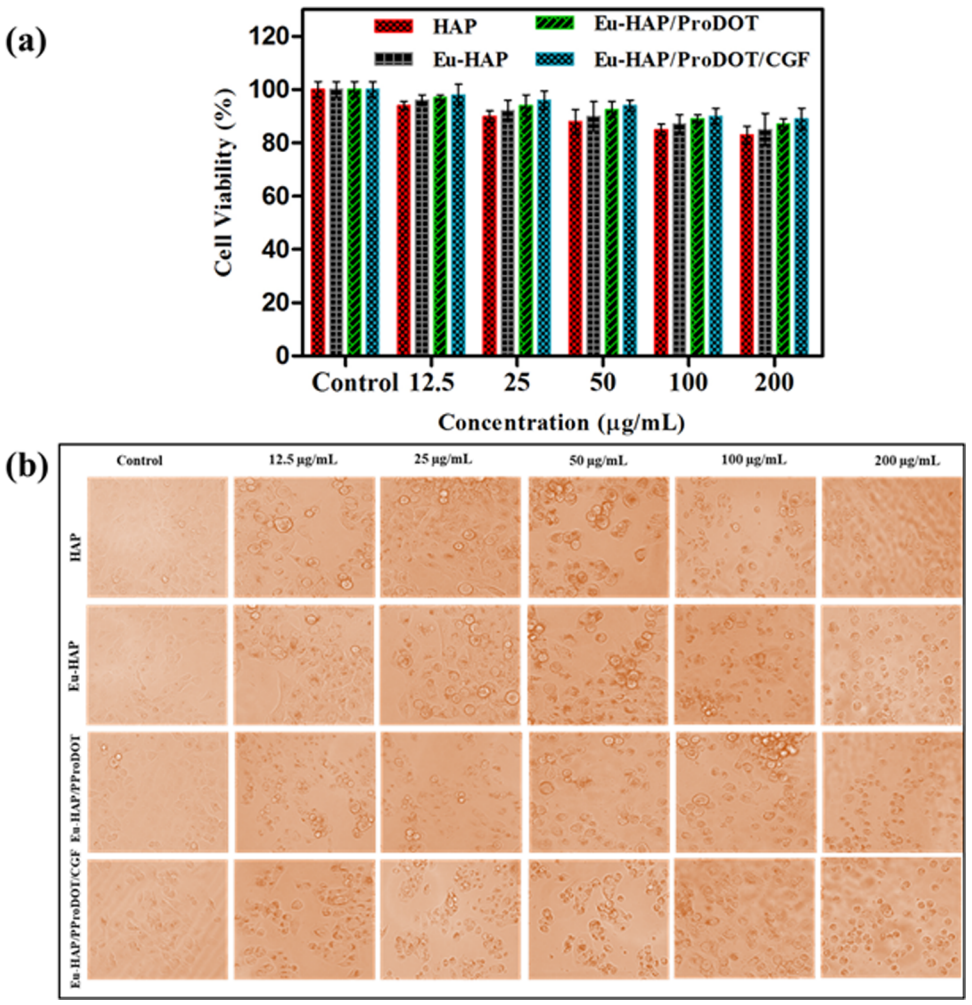

Figure 7. (a) % Cell viability and (b) optical microscopy images for the cell viability of control and different concentrations (12.5, 25, 50, 100, and 200 μg/mL) of HAP, Eu-HAP, Eu-HAP/PProDOT, and Eu-HAP/PProDOT/CGF composites at 5 days of incubation.

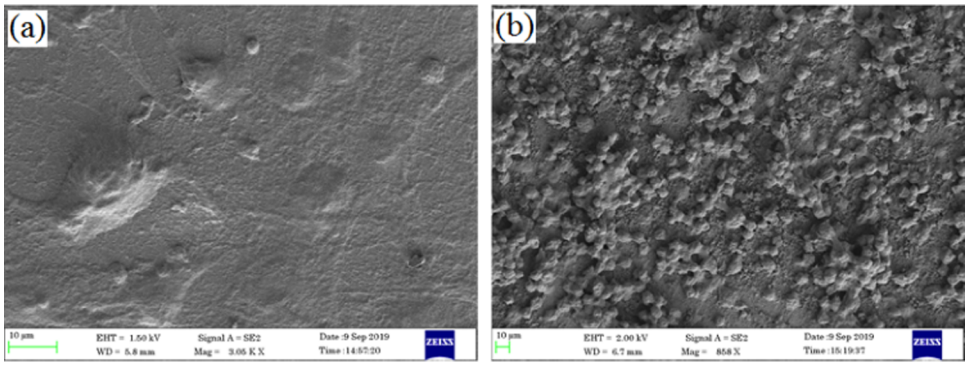

Figure 8. Surface morphology of HOS MG63 cell growth on (a) control and (b) Eu-HAP/PProDOT/CGF composite-coated Ti at 5 days of incubation.

nontoxic level (>80) of viable cells. The cell viability of the ternary composite sample is mostly due to the Eu substitution in HAP and also the presence of CGF in the Eu-HAP/PProDOT/CGF ternary composite. Thus, the as-developed Eu-HAP/PProDOT/CGF ternary composite encourages the excellent promotion of cell viability, which clearly indicates the nontoxic nature of the ternary composite for orthopedic applications. Thus, the *in vitro* cell viability study confirms the nontoxic nature of the composite, and these results validate that the Eu-HAP/PProDOT/CGF ternary composite will be an excellent composite for better biomedical applications.

Cell Adhesion. The HOS MG63 cell growth and morphology on the Eu-HAP/PProDOT/CGF ternary composite-coated Ti sample were observed using an SEM to identify the cell−material interaction and compared with control (shown in Figure 8a,b).

The enhanced cell adhesion nature of the Eu-HAP/PProDOT/CGF ternary composite at 5 days of incubation

https://doi.org/10.1021/acsomega.1c06372
ACS Omega 2022, 7, 6024−6034

clearly exhibited that the cells were adhered and spread on the Eu-HAP/PProDOT/CGF ternary composite for 5 days (Figure 8b). The Eu-HAP/PProDOT/CGF ternary composite provided important nutrients for the growth of MG63 cells. It is clearly manifested from the study that the as-developed ternary composite (Eu-HAP/PProDOT/CGF) will offer superior biocompatible nature because of the presence of CGF and the mineral Eu in HAP in the composite, which does not cause any adverse effects.

CONCLUSIONS

The multifunctional Eu-HAP/PProDOT/CGF ternary biocomposite was successfully prepared and coated on Ti via the electrophoretic deposition technique. The functional regions and diffraction patterns of the Eu-HAP/PProDOT/CGF ternary composite were slightly varied by the presence of mineral substitution in HAP, PProDOT, and CGF. The desired porelike morphology that is necessary for the growth of bone tissues is observed for the Eu-HAP /PProDOT/CGF ternary composite owing to the presence of Eu along with PProDOT and CGF. Furthermore, the antimicrobial activity and biocompatibility of the Eu-HAP/PProDOT/CGF ternary composite material along with the *in vitro* osteoblast adhesion were increased by the presence of Eu in HAP and the naturally derived CGF. The limitations of pure HAP, such as incompetent mechanical, osteogenic, and antimicrobial potential, were overcome by substituting the Eu in HAP with the combination of PProDOT along with CGF as the Eu-HAP/PProDOT/CGF ternary composite. Thus, the present study validates the suitability of the Eu-HAP/PProDOT/CGF ternary composite-coated Ti for orthopedic applications. Further, the *in vivo* studies of the as-developed Eu-HAP/PProDOT/CGF ternary composite will be carried out in the future.

EXPERIMENTAL SECTION

Chemicals. The snail shells were collected from the Cauvery river basin in Mettur dam, Salem district, Tamil Nadu, India. All chemicals and solvents, including europium nitrate pentahydrate $Eu(NO_3)_3{\cdot}5H_2O$, diammonium hydrogen phosphate $(NH_4)_2HPO_4$, 3,4-propylenedioxythiophene (ProDOT), sodium carbonate (Na_2CO_3), lithium bromide (LiBr), acetonitrile (CH_3CN), concentrated nitric acid (HNO_3), ammonium hydroxide (NH_4OH), hydrochloric acid (HCl), and sulfuric acid (H_2SO_4), were purchased from Sigma-Aldrich and used without further purification. Deionized water (DI) was used throughout the experiments.

Extraction of Calcium Oxide from Snail Shells. The snail shells were washed thoroughly under running water to remove mud and other impurities; the shells were washed again with DI several times and then boiled for 4 h at 100 °C. The snail shells were then subjected to ultrasonic treatment in an ethanol/water mixture for 2 h to remove any fibrous layer and then dried and crushed into small pieces. The dried snail shells were placed in a muffle furnace in a silica crucible and carbonized at 1000 °C for 3 h to produce calcium oxide (CaO).

Electrolyte Preparation. *Snail Shells Derived Mineral-Substituted HAP (Eu-HAP).* First, CaO (0.3 M) and $Eu(NO_3)_3{\cdot}5H_2O$ (0.1 M) were dissolved separately in DI water, and a known quantity was added in a beaker; further, 0.3 M $(NH_4)_2HPO_4$ was added dropwise to the above solution under continuous magnetic stirring at room temperature (RT) for 4 h to produce a target (Ca + Eu)/P ratio of 1.67.[46] The pH value of the suspension was adjusted to 4.5 by ammonia, and the obtained white precipitate was used for further processes.

Preparation of the Eu-HAP/PProDOT Solution. ProDOT (0.5 g) was dissolved in acetonitrile under magnetic stirring for 2 h at room temperature and then added dropwise to the above solution.[47,48] The precipitate was stirred for 12 h to obtain the electrolyte for Eu-HAP/PProDOT, which was then used for coating purposes.

Preparation of the CGF Extract and Functionalization. The soil-free CGF was collected from Kalvarayan hills, Salem, Tamil Nadu, India, and the CGF was cut into smaller pieces and washed with deionized water several times. One gram of CGF was boiled in a 0.02 M Na_2CO_3 solution for 45 min. The boiled CGF solution was collected by filtration using a Whatman filter paper and cooled. After cooling down to RT, the solution was treated with a 9.3 M LiBr solution dissolved in deionized water under magnetic stirring and warmed at 60 °C for 2 h. Finally, the resultant solution was centrifuged at 10,000 rpm, and the supernatant solution was collected and used for further processes. The solution was then subjected to functionalization by an acetylation process.

Preparation of the Ternary Composite (Eu-HAP/PProDOT/CGF). The CGF extract, as prepared in the previous section (Preparation of the CGF Extract and Functionalization), was added dropwise to the Eu-HAP/PProDOT electrolyte solution (Preparation of the Eu-HAP/PProDOT Solution) simultaneously to obtain a dirty-white precipitate. The obtained precipitate was magnetically stirred for about 24 h and then dried at 40 °C and ground into a fine powder to afford the Eu-HAP/PProDOT/CGF composite.

Preparation of Ti Specimens. The titanium specimen (99.9% purity) was cut into dimensions of 1.5 cm × 3 cm and a thickness of 0.2 mm and then embedded in an epoxy resin leaving an area of 1 cm^2 for deposition. Prior to the electrophoretic deposition of the ternary composite, the Ti specimen was polished with diverse grades of SiC emery papers (200, 400, 600, 800, and 1200 grits) and then successively rinsed with distilled water and ethanol 3−4 times. Further, it was ultrasonically cleaned in distilled water and acetone for 15 min and immediately dried in air flow. These Ti samples were used for further deposition purposes.

Electrophoretic Deposition of the Eu-HAP/PProDOT/CGF Ternary Composite on Ti. The as-prepared ternary composite was dissolved in 50 mL of ethanol/water mixture for the deposition process. The suspension was stirred well using a magnetic stirrer for 1 h and then further dispersed ultrasonically for about 2 h to ensure uniform dispersion of the ternary composite. The deposition was carried out at room temperature only using a DC power supply with a two-electrode system.[49] The Ti metal served as the working electrode (cathode) and the platinum electrode was used as the anode, placed at a distance of 3 cm apart, and these electrodes were placed in the beaker containing composite suspension. The deposition was carried out by applying a constant voltage of 20 V for 10 min. The deposition condition was obtained by the trial-and-error approach to obtain the desired and uniform coating through visual inspections. After each deposition, the coated Ti metals were carefully pulled out of the suspension and dried for 24 h and then stored in a desiccator at room temperature.

https://doi.org/10.1021/acsomega.1c06372
ACS Omega 2022, 7, 6024−6034

Characterization Techniques. *Structural Characterizations.* The Fourier transform infrared spectra (FTIR) were recorded using an FTIR, Impact 400 D Nicolet spectrometer, with the frequency ranging from 4000 to 500 cm^{-1} with 32 scans and a spectral resolution of 4 cm^{-1} for the evaluation of the functional groups present in the ternary composite. The composite coating was scraped carefully from the Ti metal and then made into pellets by mixing with KBr and used for evaluation. The phase composition of the ternary composite coatings was performed using the X-ray diffraction (XRD) technique using a PANalytical X'Pert PRO diffractometer in the 2θ range of 10−80° at a scan rate of 0.02° with Cu Kα radiation (1.5406 Å).

Morphological Characterizations. The surface morphology of the as-developed coatings was observed using a field emission scanning electron microscope (FE-SEM, JSM 840A scanning microscope operating with an accelerating voltage of 30.0 kV). The different elemental compositions of the ternary composite were examined by energy-dispersion spectroscopy (EDX).

Mechanical Characterization. The adhesion strength of the coatings over Ti was calculated by a pull-out test using a Universal Instron Mechanical Testing system (Instron 5565, Instron Co.), according to the ASTM F 1044-05 standard at a cross-head speed of 1 mm min^{-1} with at least five measurements for each ternary composite-coated Ti.[50] Also, the hardness of coatings was tested using an Akashi AAV-500 series hardness tester five times, and the hardness values for the coating were an average of five different hardness test measurements.

Electrochemical Characterizations. The potentiodynamic polarization measurements were recorded in a simulated body fluid (SBF) solution to examine the corrosion protection performance of the ternary composite coatings.[51] For this purpose, a three-electrode cell assembly (i.e., a saturated calomel electrode (SCE), platinum electrode, and Ti specimens were used as the reference, counter, and working electrodes, respectively), and the CHI 760C electrochemical workstation was used for measurements. The potentiodynamic polarization measurements were measured at a scan rate of 1 $mV{\cdot}s^{-1}$ between the potential range of −0.5 and 0.5 V. The data thus obtained were recorded using internally available software, and each experiment was repeated three times to check reproducibility.

Biological Characterizations. The *in vitro* antibacterial activity of the HAP, Eu-HAP, Eu-HAP/PProDOT, and Eu-HAP/PProDOT/CGF ternary composite coatings was evaluated by the well diffusion method against two bacterial strains, i.e., Gram-positive, *Staphylococcus aureus* (*S. aureus*) and Gram-negative, *Escherichia coli* (*E. coli*), by adopting the procedure as reported earlier.[52] These bacterial strains are the most common pathogens associated with bone infections, and hence, they are found suitable for estimating the antibacterial properties of the ternary composite coatings on Ti. For this purpose, 20 g/L concentration of agar medium was used as a nutrient to induce the growth of bacteria. The microbial stock solution was prepared by the overnight growth of *S. aureus* and *E. coli* in tryptic soy broth at RT with constant stirring. Muller−Hinton agar was used for the test and was carried out by pouring the agar into the petri dish to form a 4 mm thick layer. Then, to obtain the semiconfluent growth, 2 mL of dense inoculums of the microorganism was added. The petri dish was left to dry for 10 min, and then the two different volume concentrations (50 and 100 μg/mL) of HAP, Eu-HAP, Eu-HAP/PProDOT, and Eu-HAP/PProDOT/CGF ternary composite coatings were added into the well in the petri dish containing nutrient agar and then incubated for 24 h at 37 °C. After the incubation, the antibacterial activity of the coatings was measured by the diameters (mm) of the growth inhibition zone.

The biocompatibility of the Eu-HAP/PProDOT/CGF ternary composite (at different concentrations of 12.5, 25, 50, 100, 200 μg/mL) was evaluated against the Human osteosarcoma MG63 cells (HOS MG63, ATCC CRL-1427TM) by the MTT assay test. The cells were purchased from NCCL, Pune. The purchased cells were maintained in Dulbecco's modified Eagle medium (DMEM, GIBCO) supplemented with 10% FBS and 1% antibiotic solution at 37 °C in a humidified atmosphere of 5% CO_2. The cultured cells were then seeded onto the ternary composite samples with a density of 5×10^4 cells cm^{-2} in 24-well plates. The cells in 24-well plates at the same seeding density without the samples were used as control. To determine the cytotoxicity, the cell viability (as a percentage) was calculated, with respect to the control,[53] as

$$\%\text{cell viability} = [A]\text{test}/[A]\text{control} \times 100$$

To determine the cell−surface interaction, the cell adhesion test was performed with HOS MG 63 cells for the Eu-HAP/PProDOT/CGF ternary composite coating on Ti. The cells were grown on the Dulbecco's modified Eagle medium (DMEM) supplemented with 10% FBS and 1% penicillin/streptomycin.[54] The coated samples were sterilized, and the cells at a density of 5×10^5 mL^{-1} were seeded on them and then incubated in a CO_2 incubator with the standard culture condition; the well without the samples was used as control. After an interval of 2 days, the culture medium was removed and then replaced with fresh culture medium into each well. Then, after a stipulated time period, the ternary composite-coated sample was washed with phosphate-buffered saline. Further, for the SEM morphological observation, the seeded samples were fixed with 2% glutaraldehyde and then dehydrated with the ethanol/water mixture for 10 min. To preserve the original morphology of the cells, 0.5 mL of hexamethyldisilazane (HMDS, HiMedia) was added to each well. Further, the samples were coated with gold prior to the SEM observation.

Statistical Analysis. The experiments involved in this study were performed in triplicate using statistical analysis by a one-factor statistical study (ANOVA; Tukey's test for a post hoc examination), and their corresponding experimental data were given in average ± standard deviation. The difference between the samples was observed to be statistically significant with $p < 0.05$.

AUTHOR INFORMATION

Corresponding Author

Gopi Dhanaraj − *Department of Chemistry, Periyar University, Salem 636011 , Tamil Nadu, India;* orcid.org/0000-0001-6662-1238; Email: dhanaraj_gopi@yahoo.com

Authors

Ramachandran Raji − *Department of Chemistry, Periyar University, Salem 636011 , Tamil Nadu, India*

https://doi.org/10.1021/acsomega.1c06372
ACS Omega 2022, 7, 6024−6034

Shinyjoy Elangomannan − *Department of Physics, School of Basic and Applied Sciences, Central University of Tamil Nadu, Thiruvarur 610101 , Tamil Nadu, India*
Ramya Subramani − *Department of Physics, School of Basic and Applied Sciences, Central University of Tamil Nadu, Thiruvarur 610101 , Tamil Nadu, India*
Kavitha Louis − *Department of Physics, School of Basic and Applied Sciences, Central University of Tamil Nadu, Thiruvarur 610101 , Tamil Nadu, India*
Manoravi Periasamy − *Materials Chemistry and Metal Fuel Cycle Group, Indira Gandhi Centre for Atomic Research, Kalpakkam 603102 , Tamil Nadu, India*

Complete contact information is available at: https://pubs.acs.org/10.1021/acsomega.1c06372

Notes

The authors declare no competing financial interest.

■ ACKNOWLEDGMENTS

G.D. acknowledges the major financial support from the Department of Science and Technology (DST-SERB, ref No.: EMR/2017/003803) and University Grants Commission-Department of Atomic energy (UGC-DAE CSR, ref No. CSR-KN/CRS-118/2018-19/1056). R.R. acknowledges Periyar University for University Research Fellowship (ref No.: PU/AD-3/URF/027232/2019). S.E. (F.4-2/2006 (BSR)/CH/18-19/0078, Dated: 06.02.2019) and R.S. (F.4-2/2006(BSR)/CH/17-18/0170, Dated: 25.09.2018) acknowledges the University Grants Commission for Dr. D.S. Kothari Fellowship, New Delhi, India.

■ REFERENCES

(1) Lems, W. F.; Raterman, H. G. Critical Issues and Current Challenges in Osteoporosis and Fracture Prevention. An Overview of Unmet Needs. *Ther. Adv. Musculoskelet. Dis.* **2017**, *9*, 299−316.
(2) Xie, Y.; Zhang, L.; Xiong, Q.; Gao, Y.; Ge, W.; Tang, P. Bench-to-Bedside Strategies for Osteoporotic Fracture: From Osteoimmunology to Mechanosensation. *Bone Res.* **2019**, *7*, No. 25.
(3) Calori, G. M.; Mazza, E.; Colombo, M.; Ripamonti, C. The Use of Bone-Graft Substitutes in Large Bone Defects: Any Specific Needs? *Injury* **2011**, *42*, S56−S63.
(4) Liu, Y.; Lim, J.; Teoh, S.-H. Review: Development of Clinically Relevant Scaffolds for Vascularised Bone Tissue Engineering. *Biotechnol. Adv.* **2013**, *31*, 688−705.
(5) Deng, Y.; Sun, Y.; Bai, Y.; Gao, X.; Zhang, H.; Xu, A.; Huang, E.; Deng, F.; Wei, S. In Vitro Biocompability/Osteogenesis and In Vivo Bone Formation Evalution of Peptide-Decorated Apatite Nanocomposites Assisted via Polydopamine. *J. Biomed. Nanotechnol.* **2016**, *12*, 602−618.
(6) Prasad, K.; Bazaka, O.; Chua, M.; Rochford, M.; Fedrick, L.; Spoor, J.; Symes, R.; Tieppo, M.; Collins, C.; Cao, A.; Markwell, D.; Ostrikov, K.Ken.; Bazaka, K. Metallic Biomaterials: Current Challenges and Opportunities. *Materials* **2017**, *10*, 884.
(7) Feng, X. Chemical and Biochemical Basis of Cell-Bone Matrix Interaction in Health and Disease. *Curr. Chem. Biol.* **2009**, *3*, 189−196.
(8) Lin, X.; Patil, S.; Gao, Y.-G.; Qian, A. The Bone Extracellular Matrix in Bone Formation and Regeneration. *Front. Pharmacol.* **2020**, *11*, No. 757.
(9) Fang, J.; Li, P.; Lu, X.; Fang, L.; Lü, X.; Ren, F. A Strong, Tough, and Osteoconductive Hydroxyapatite Mineralized Polyacrylamide/dextran Hydrogel for Bone Tissue Regeneration. *Acta Biomater.* **2019**, *88*, 503−513.
(10) Balu, S. K.; Sampath, V.; Andra, S.; Alagar, S.; Manisha Vidyavathy, S. Fabrication of Carbon and Silver Nanomaterials Incorporated Hydroxyapatite Nanocomposites: Enhanced Biological and Mechanical Performances for Biomedical Applications. *Mater. Sci. Eng., C* **2021**, *128*, No. 112296.
(11) Yan, D.; Lou, Y.; Han, Y.; Wickramaratne, M. N.; Dai, H.; Wang, X. Controllable Synthesis of Poly(acrylic Acid)-Stabilized Nano-Hydroxyapatite Suspension by an Ultrasound-Assisted Precipitation Method. *Mater. Lett.* **2018**, *227*, 9−12.
(12) Arun Prakash, V. C.; Venda, I.; Thamizharasi, V.; Sathya, E. A New Attempt on Synthesis of Spherical Nano Hydroxyapatite Powders Prepared by Dimethyl Sulfoxide - Poly Vinyl Alcohol Assisted Microemulsion Method. *Mater. Chem. Phys.* **2021**, *259*, No. 124097.
(13) Ansari, Z.; Kalantar, M.; Kharaziha, M.; Ambrosio, L.; Raucci, M. G. Polycaprolactone/fluoride Substituted-Hydroxyapatite (PCL/FHA) Nanocomposite Coatings Prepared by in-Situ Sol-Gel Process for Dental Implant Applications. *Prog. Org. Coat.* **2020**, *147*, No. 105873.
(14) Mohd Pu'ad, N.A.S.; Koshy, P.; Abdullah, H. Z.; Idris, M. I.; Lee, T. C. Syntheses of Hydroxyapatite from Natural Sources. *Heliyon* **2019**, *5*, No. e01588.
(15) Anjaneyulu, U.; Pattanayak, D. K.; Vijayalakshmi, U. Snail Shell Derived Natural Hydroxyapatite: Effects on NIH-3T3 Cells for Orthopedic Applications. *Mater. Manuf. Process* **2016**, *31*, 206−216.
(16) Chen, J.; Wen, Z.; Zhong, S.; Wang, Z.; Wu, J.; Zhang, Q. Synthesis of Hydroxyapatite Nanorods from Abalone Shells via Hydrothermal Solid-State Conversion. *Mater. Des.* **2015**, *87*, 445−449.
(17) Khiri, M. Z. A.; Matori, K. A.; Zainuddin, N.; Abdullah, C. A. C.; Alassan, Z. N.; Baharuddin, N. F.; Zaid, M. H. M. The Usability of Ark Clam Shell (Anadara Granosa) as Calcium Precursor to Produce Hydroxyapatite Nanoparticle via Wet Chemical Precipitate Method in Various Sintering Temperature. *SpringerPlus* **2016**, *5*, No. 1206.
(18) Pooladi, A.; Bazargan-Lari, R. Simultaneous Removal of Copper and Zinc Ions by Chitosan/Hydroxyapatite/nano-Magnetite Composite. *J. Mater. Res. Technol.* **2020**, *9*, 14841−14852.
(19) Xu, X.; Wang, N.; Wu, M.; Wang, J.; Wang, D.; Chen, Z.; Xie, J.; Ding, C.; Li, J. Programmed Antibacterial and Mineralization Therapy for Dental Caries Based on Zinc-Substituted Hydroxyapatite/ Alendronate-Grafted Polyacrylic Acid Hybrid Material. *Colloids Surf., B* **2020**, *194*, No. 111206.
(20) Gopi, D.; Shinyjoy, E.; Kavitha, L. Synthesis and Spectral Characterization of Silver/magnesium Co-Substituted Hydroxyapatite for Biomedical Applications. *Spectrochim. Acta, Part A* **2014**, *127*, 286−291.
(21) Veljovic, D.; Matic, T.; Stamenic, T.; Kojic, V.; Dimitrijevic-Brankovic, S.; Lukic, M. J.; Jevtic, S.; Radovanovic, Z.; Petrovic, R.; Janackovic, D. Mg/Cu Co-Substituted Hydroxyapatite − Biocompatibility, Mechanical Properties and Antimicrobial Activity. *Ceram. Int.* **2019**, *45*, 22029−22039.
(22) Morais, D. S.; Coelho, J.; Ferraz, M. P.; Gomes, P. S.; Fernandes, M. H.; Hussain, N. S.; Santos, J. D.; Lopes, M. A. Samarium Doped Glass-Reinforced Hydroxyapatite with Enhanced Osteoblastic Performance and Antibacterial Properties for Bone Tissue Regeneration. *J. Mater. Chem. B* **2014**, *2*, 5872−5881.
(23) Chen, Y.; Zhang, Y. Q.; Zhang, T. H.; Gan, C. H.; Zheng, C. Y.; Yu, G. Carbon Nanotube Reinforced Hydroxyapatite Composite Coatings Produced through Laser Surface Alloying. *Carbon* **2006**, *44*, 37−45.
(24) Kumar, A.; Biswas, K.; Basu, B. On the Toughness Enhancement in Hydroxyapatite-Based Composites. *Acta Mater.* **2013**, *61*, 5198−5215.
(25) Balint, R.; Cassidy, N. J.; Cartmell, S. H. Conductive Polymers: Towards a Smart Biomaterial for Tissue Engineering. *Acta Biomater.* **2014**, *10*, 2341−2353.
(26) Mazaheripour, A.; Thomas, E. M.; Segalman, R. A.; Chabinyc, M. L. Nonaggregating Doped Polymers Based on Poly(3,4-Propylenedioxythiophene). *Macromolecules* **2019**, *52*, 2203−2213.

(27) Strakosas, X.; Wei, B.; Martin, D. C.; Owens, R. M. Biofunctionalization of Polydioxythiophene Derivatives for Biomedical Applications. *J. Mater. Chem. B* **2016**, *4*, 4952−4968.
(28) Kenry; Liu, B. Recent Advances in Biodegradable Conducting Polymers and Their Biomedical Applications. *Biomacromolecules* **2018**, *19*, 1783−1803.
(29) Qiu, D.; Yang, L.; Yin, Y.; Wang, A. Preparation and Characterization of Hydroxyapatite/titania Composite Coating on NiTi Alloy by Electrochemical Deposition. *Surf. Coat. Technol.* **2011**, *205*, 3280−3284.
(30) Catauro, M.; Papale, F.; Bollino, F. Characterization and Biological Properties of TiO2/PCL Hybrid Layers Prepared via Sol−gel Dip Coating for Surface Modification of Titanium Implants. *J. Non. Cryst. Solids* **2015**, *415*, 9−15.
(31) Qiu, D.; Wang, A.; Yin, Y. Characterization and Corrosion Behavior of Hydroxyapatite/zirconia Composite Coating on NiTi Fabricated by Electrochemical Deposition. *App. Surf. Sci.* **2010**, *257*, 1774−1778.
(32) Janković, A.; Eraković, S.; Vukašinović-Sekulić, M.; Mišković-Stanković, V.; Park, S. J.; Rhee, K. Y. Graphene-Based Antibacterial Composite Coatings Electrodeposited on Titanium for Biomedical Applications. *Prog. Org. Coat.* **2015**, *83*, 1−10.
(33) Sarkar, C.; Sahu, S. K.; Sinha, A.; Chakraborty, J.; Garai, S. Facile Synthesis of Carbon Fiber Reinforced Polymer-Hydroxyapatite Ternary Composite: A Mechanically Strong Bioactive Bone Graft. *Mater.Sci. Eng., C* **2019**, *97*, 388−396.
(34) Zhu, Y.; Wang, Z.; Zhou, H.; Li, L.; Zhu, Q.; Zhang, P. An Injectable Hydroxyapatite/poly(lactide-Co-Glycolide) Composite Reinforced by Micro/nano-Hybrid Poly(glycolide) Fibers for Bone Repair. *Mater. Sci. Eng., C* **2017**, *80*, 326−334.
(35) Sarkar, C.; Sahu, S. K.; Sinha, A.; Chakraborty, J.; Garai, S. Facile Synthesis of Carbon Fiber Reinforced Polymer-Hydroxyapatite Ternary Composite: A Mechanically Strong Bioactive Bone Graft. *Mater. Sci. Eng., C* **2019**, *97*, 388−396.
(36) Mahar, R.; Dixit, S.; Joshi, T.; Kanojiya, S.; Mishra, D. K.; Konwar, R.; Shukla, S. K. Bioactivity Guided Isolation of Oxypregnane-Oligoglycosides (Calotroposides) from the Root Bark of *Calotropis Gigantea* as Potent Anticancer Agents. *RSC Adv.* **2016**, *6*, 104215−104226.
(37) Ashori, A.; Bahreini, Z. Evaluation of *Calotropis Gigantea* as a Promising Raw Material for Fiber-Reinforced Composite. *J. Compos. Mater.* **2009**, *43*, 1297−1304.
(38) Babu, G. D.; Babu, K. S.; Kishore, P. N. Tensile and Wear Behavior of *Calotropis Gigentea* Fruit Fiber Reinforced Polyester Composites. *Procedia Eng.* **2014**, *97*, 531−535.
(39) Ramasamy, R.; Obi Reddy, K.; Varada Rajulu, A. Extraction and Characterization of *Calotropis Gigantea* Bast Fibers as Novel Reinforcement for Composites Materials. *J. Nat. Fibers* **2018**, *15*, 527−538.
(40) Velusamy, K.; Navaneethakrishnan, P.; Rajeshkumar, G.; Sathishkumar, T. The Influence of Fiber Content and Length on Mechanical and Water Absorption Properties of *Calotropis Gigantea* Fiber Reinforced Epoxy Composites. *J. Ind. Text.* **2019**, *48*, 1274−1290.
(41) Yin, X.; Yan, L.; Jun Hao, D.; Liu, S.; Yang, M.; He, B.; Liu, Z. Calcium Alginate Template-Mineral Substituted Hydroxyapatite Hydrogel Coated Titanium Implant for Tibia Bone. *Regeneration Int. J. Pharm.* **2020**, *582*, No. 119303.
(42) Singh, S.; Singh, G.; Bala, N. Electrophoretic Deposition of Hydroxyapatite-Iron Oxide-Chitosan Composite Coatings on Ti−13Nb−13Zr Alloy for Biomedical Applications. *Thin Solid Films* **2020**, *697*, No. 137801.
(43) Gopi, D.; Karthika, A.; Rajeswari, D.; Kavitha, L.; Pramod, R.; Dwivedi, J. Investigation on Corrosion Protection and Mechanical Performance of Minerals Substituted Hydroxyapatite Coating on HELCDEB-Treated Titanium Using Pulsed Electrodeposition Method. *RSC Adv.* **2014**, *4*, 34751−34759.
(44) Ratha, I.; Datta, P.; Balla, V. K.; Nandi, S. K.; Kundu, B. Effect of Doping in Hydroxyapatite as Coating Material on Biomedical Implants by Plasma Spraying Method: A Review. *Ceram. Int.* **2021**, *47*, 4426−4445.
(45) Surmenev, R. A.; Grubova, I. Y.; Neyts, E.; Teresov, A. D.; Koval, N. N.; Epple, M.; Tyurin, A. I.; Pichugin, V. F.; Chaikina, M. V.; Surmeneva, M. A. Ab Initio Calculations and a Scratch Test Study of RF-Magnetron Sputter Deposited Hydroxyapatite and Silicon-Containing Hydroxyapatite Coatings. *Surf. Interfaces* **2020**, *21*, No. 100727.
(46) Sathishkumar, S.; Louis, K.; Shinyjoy, E.; Gopi, D. Tailoring the Sm/Gd-Substituted Hydroxyapatite Coating on Biomedical AISI 316L SS: Exploration of Corrosion Resistance, Protein Profiling, Osteocompatibility, and Osteogenic Differentiation for Orthopedic Implant Applications. *Ind. Eng. Chem. Res.* **2016**, *55*, 6331−6344.
(47) Siju, C. R.; Saravanan, T. R.; Rao, K. N.; Sindhu, S. Optical, Electrochemical, and Structural Properties of Spray Coated Dihexyl Substituted Poly (3,4 Propylene Dioxythiophene) Film for Optoelectronics Devices. *Int. J. Polym. Mater.* **2014**, *63*, 374−379.
(48) Jäger, M.; Zilkens, C.; Zanger, K.; Krauspe, R. Significance of Nano- and Microtopography for Cell-Surface Interactions in Orthopaedic Implants. *J. Biomed. Biotechnol.* **2007**, *2007*, 1−19.
(49) Gopi, D.; Nithiya, S.; Shinyjoy, E.; Rajeswari, D.; Kavitha, L. Carbon Nanotubes/Carboxymethyl Chitosan/Mineralized Hydroxyapatite Composite Coating on Ti-6Al-4V Alloy for Improved Mechanical and Biological Properties. *Ind. Eng. Chem. Res.* **2014**, *53*, 7660−7669.
(50) Zarr, R. R.; Bruss, S. M.; McElroy, D. L. Historical Review of the Metered Section Area for the Guarded-Hot-Plate Method. *J. Test. Eval.* **2019**, *47*, No. 20180652.
(51) Gopi, D.; Kanimozhi, K.; Bhuvaneshwari, N.; Indira, J.; Kavitha, L. Novel Banana Peel Pectin Mediated Green Route for the Synthesis of Hydroxyapatite Nanoparticles and Their Spectral Characterization. *Spectrochim. Acta, Part A* **2014**, *118*, 589−597.
(52) Rajeswari, D.; Gopi, D.; Ramya, S.; Kavitha, L. Investigation of Anticorrosive, Antibacterial and in Vitro Biological Properties of a Sulphonated Poly(etheretherketone)/strontium, Cerium Co-Substituted Hydroxyapatite Composite Coating Developed on Surface Treated Surgical Grade Stainless Steel for Orth. *RSC. Adv.* **2014**, *4*, 61525−61536.
(53) Gopi, D.; Ramya, S.; Rajeswari, D.; Surendiran, M.; Kavitha, L. Development of Strontium and Magnesium Substituted Porous hydroxyapatite/poly(3,4-Ethylenedioxythiophene) Coating on Surgical Grade Stainless Steel and Its Bioactivity on Osteoblast Cells. *Colloids Surf., B* **2014**, *114*, 234−240.
(54) Sun, J.; Zheng, X.; Li, H.; Fan, D.; Song, Z.; Ma, H.; Hua, X.; Hui, J. Monodisperse Selenium-Substituted Hydroxyapatite: Controllable Synthesis and Biocompatibility. *Mater. Sci. Eng., C* **2017**, *73*, 596−602.
(55) Ganeshan, P.; NagarajaGanesh, B.; Ramshankar, P.; Raja, K. *Calotropis Gigantea* Fibers: A Potential Reinforcement for Polymer Matrices. *Int. J. Polym. Anal. Charact.* **2018**, *23*, 271−277.
(56) Sun, R.; Kezheng, C.; Xiangfeng, W.; Dandan, Z.; Zhenzong, S. Controlled synthesis and enhanced luminescence of europium-doped fluorine-substituted hydroxyapatite nanoparticles. *CrystEngComm* **2013**, *15*, 3442−3447.
(57) Gopi, D.; Sathishkumar, S.; Karthika, A.; Kavitha, L. Development of Ce^{3+}/Eu^{3+} Dual Substituted Hydroxyapatite Coating on Surgical Grade Stainless Steel for Improved Antimicrobial and Bioactive Properties. *Ind. Eng. Chem. Res.* **2014**, *53*, 20145−20153.
(58) Karazehir, T.; Sarac, B.; Gilsing, H.-D.; Eckert, J.; Sarac, A. S. Oligoether Ester-Functionalized ProDOT Copolymers on Si/Monolayer Graphene as Capacitive Thin Film Electrodes. *J. Electrochem. Soc.* **2020**, *167*, No. 070543.

https://doi.org/10.1021/acsomega.1c06372
ACS Omega 2022, 7, 6024−6034